Available online at www.sciencedirect.com
SCIENCE DIRECT®
Journal of Sound and Vibration 292 (2006) 279–299
JOURNAL OF SOUND AND VIBRATION
www.elsevier.com/locate/jsvi

Controlled vortex-induced vibration on a fix-supported flexible cylinder in cross-flow

L. Cheng*, Y. Zhou, M.M. Zhang

Department of Mechanical Engineering, The Hong Kong Polytechnic University, Hung Hom, Kowloon, Hong Kong

Received 15 March 2004; received in revised form 9 June 2005; accepted 29 July 2005
Available online 21 September 2005

Abstract

This paper presents an experimental study on the closed-loop control of the vortex-induced vibration of a flexible square cylinder, fixed at both ends, in a cross-flow. Curved piezoceramic actuators were embedded underneath one cylinder surface to generate a controllable motion to perturb the interaction between flow and structure. Five control schemes were investigated based on the feedback from either individual or combined responses of structural vibration and fluctuating flow. Experiments were conducted in the first-mode resonance of the cylinder, when the vortex-shedding frequency coincided with the first-mode natural frequency of the fluid–structure system. The control effect on the structural vibration and the flow was simultaneously monitored using laser vibrometer, optical fiber Bragg grating (FBG) sensor, hot wires, particle image velocimetry, laser-induced fluorescence flow visualization and laser Doppler anemometer. The performances of the different schemes were assessed and compared. The best performance was achieved using the scheme whose feedback signal was a combination of flow and structural vibration. Vortex shedding was almost completely destroyed, resulting in a reduction by 85% in the vortex strength, by 71% in the structural vibration amplitude, and by 30% in the drag coefficient. It was found that the control effect altered the nature of the fluid–structure interactions, changing the in-phased fluid–structure synchronization into anti-phased interactions, thus significantly enhancing the damping of the fluid–structure system and contributing to greatly attenuated vortex shedding and the structural vibration.

*Corresponding author. Tel.: +852 2766 6769; fax: +852 2365 4703.
E-mail address: mmlcheng@polyu.edu.hk (L. Cheng).

0022-460X/$ - see front matter © 2005 Elsevier Ltd. All rights reserved.
doi:10.1016/j.jsv.2005.07.044

1. Introduction

A cross-flow blowing over bluff bodies is usually unsteady. Beyond a critical Reynolds number ($Re = U_\infty h/v$, where U_∞ is the free-stream velocity, h is the characteristic height of the body and v is the kinematic viscosity), the boundary layer will separate from each side of the body to form the so-called Kármán vortex street. The alternately shed vortices from the body generate periodic forces on the structure, causing a structural vibration. The structural motion in turn influences the flow field, giving rise to nonlinear fluid–structure interaction [1]. The phenomenon is quite common in engineering such as underwater pipelines, chimney stacks, bridges and high-rise buildings, and may have a dramatic impact on the fatigue life of the structures in the long run, even leading to disastrous consequences. Vortex shedding and vortex-induced vibration are also responsible for noise generations [2]. Naturally, the control of vortex shedding and vortex-induced structural vibration has attracted a great attention in the literature [3].

Both passive and active controls have been investigated in the past. Passive methods require no external energy input, typically changing the cross-section of structures, adding fixed mechanical vortex disturbers, longitudinal grooves or riblets to influence vortex shedding [4–6]. Active schemes can be either open or closed-loop, both involving energy input to a flow–structure system via actuators or other means to bring about desirable changes to the system. The former uses independent external control signals, whereas the latter relies on a feedback signal from the system. In the category of open-loop control, Hsiao and Shyu [7] used acoustic waves emitted from a slot on the surface of a cylinder to disturb the fluid field and demonstrated that a local disturbance near the shear layer instability frequency and around the flow separation point caused an increase in lift but a reduction in drag and the vortex scale ($Re = 420$–$34\,000$). Williams et al. [8] introduced symmetric and anti-symmetric forcing into a water flow ($Re = 470$) at a frequency of about two times the vortex-shedding frequency (f_s) through two rows of holes located at $\pm 45^\circ$, respectively, away from the forward stagnation line of the cylinder. They observed a modified behavior of f_s and the flow structure.

Most of existing closed-loop methods rely on feedback signals provided by hot wires in the turbulent wake for the vortex shedding control. Warui and Fujisawa [9] reduced the vortex strength at $Re = 6700$ using electromagnetic actuators installed at both ends of a circular cylinder to create a lateral oscillation. Tokumaru and Dimotakis [10] and Filler et al. [11] created a rotary oscillation of a cylinder to produce regulated injection of circulation into the wake, both leading to an attenuation in the vortex strength and drag force. Ffowcs Williams and Zhao [12] controlled a loudspeaker mounted on a wind tunnel wall to impair vortex shedding from a cylinder at $Re = 400$. Roussopoulos [13] revisited the problem using the same technique and reported an increase in the onset Reynolds number for vortex shedding by 20%. Huang [14] used sound generated inside a cylinder through a thin slit near the separation point on the cylinder surface and observed that the vortex shedding on both sides of the cylinder could be suppressed in a Re range between 4×10^3 and 1.3×10^4.

Another approach is to control directly the vortex-induced structural vibration. Baz and Kim [15] used an electromagnetic actuator installed inside a cantilevered flexible cylinder to exert a force on the cylinder. Based on the feedback information on the cylinder vibration, piezoelectric actuators generated a control action to attenuate the vortex-induced vibration at the first-mode resonance. As a result, the amplitude of vibration was reduced by 40% over a Re range between

5500 and 7500. Their work entirely focused on vibration control. No information on the flow was provided since the flow was considered as a disturbance rather than a control target.

Previous research focused on a separate control of either fluid field or structural vibration. Many engineering applications, however, require the simultaneous control of both. As a matter of fact, the simultaneous control of both can be more effective. Cheng et al. [16] proposed a perturbation technique using curved piezoceramic actuators embedded underneath the surface of a square cylinder. Open-loop control tests showed that both fluid field and structural vibration can be controlled given the appropriate tuning of the perturbation frequency. The technique was further expanded to a closed-loop control system in Zhang et al. [17]. It was found that the best performance was achieved in terms of both suppressing vortex shedding and its induced vibration provided that feedback signal was properly chosen.

Apart from Baz and Kim [15], all aforementioned work examined rigid cylinders, either fixedly or flexibly supported. In practice, however, engineering structures are frequently flexible. Problems related to fatigue or noise radiation are mainly related to the flexural vibration of these structures, especially at the occurrence of resonances, when the vortex-shedding frequency coincided with one of the natural frequencies of the system. The study of the structural resonances of lower modes (the 1st mode in particular) is of particular importance due to the large vibration amplitude involved. The technique proposed in Refs. [16,17] owns its effectiveness to a spanwise uniform perturbation created by actuators. Since flexible structures undergo non-uniform flexural vibrations along the spanwise direction, the effectiveness of this technique needs re-assessing. Meanwhile, the best control scheme has to be identified among the multitudinous combinations of feedback signals.

This work aims to address the issues raised above. Closed-loop control of vortex shedding and vortex-induced vibration of a fix-supported flexible square cylinder under the resonance condition was experimentally investigated. Five control schemes were considered and compared, which utilized feedback signals from streamwise fluctuating flow velocity u, lateral structural vibration Y, dynamic strain ε_y caused by the vibration, or a combination of these responses. These signals were measured using a hot wire, a laser vibrometer and an optical fiber Bragg grating (FBG) sensor, respectively. The control performances on the structural oscillation were evaluated in both time and frequency domain of Y, ε_y and u. In order to understand the underlying physics, the flow behind the cylinder was documented using a number of techniques, including particle image velocimetry (PIV), laser-induced fluorescence (LIF) flow visualization and a two-component laser Doppler anemometer (LDA). The spectral phase and coherence between u and Y, along with the varying damping of the fluid–structure system under the control, were discussed in detail.

2. Experimental details

2.1. Principle of the perturbation technique

Vortex shedding from a bluff body results from the initially linear wake instability [18]. The mature vortex structure depends on its infant form and a small local perturbation near the separation point will grow and exert significant influence on the unsteady Kármán vortex structure. Although, the physics behind is not fully understood, there are strong evidences that

weak perturbations do influence vortex shedding in the highly nonlinear unsteady wake, and this influence can be dramatic. Since vortex shedding and its induced vibration are coupled, a properly introduced perturbation may be expected to alter the nature of fluid–structure interaction, achieving the simultaneous impairment of both vortex shedding and structural vibration. Based on this idea, the perturbation technique used in this paper creates a local perturbation on the structural surface by embedding piezoceramic actuators inside the structure so as to modify the interaction between flow and structural vibration.

2.2. Experimental setup

Experiments were carried out in a closed-circuit wind tunnel with a square working section 0.6 m × 0.6 m and 2.4 m long [19]. A flexible square cylinder, made of nylon, with a height $h = 17.3$ mm was fix-supported at both ends and placed 0.2 m downstream of the exit plane of the tunnel contraction, as shown in Fig. 1. Curved THUNDER (THin layer composite UNimorph piezoelectric Driver and sEnsoR) actuators, developed by NASA Langley research center [20], were used as actuators. Under an applied voltage, the actuator deforms out of plane. Due to its special fabrication process and the effect of curvature, THUNDER actuator is superior to traditional pizeoceramic actuators in many aspects such as large displacement and reasonably good load-bearing capacity. Without any loading, the actuator used in this work may generate a maximum displacement of about 2 mm and a frequency up to 2 kHz. Three THUNDER actuators were installed in series between the slot on the top of the cylinder and a plastic plate (see the cut-away view in Fig. 1). The plastic plate was flushed with the cylinder surface. Driven by the actuators, the plastic plate moved up and down to provide the desired perturbation. The detailed information on the installation of the actuators was described in Cheng et al. [16]. At the

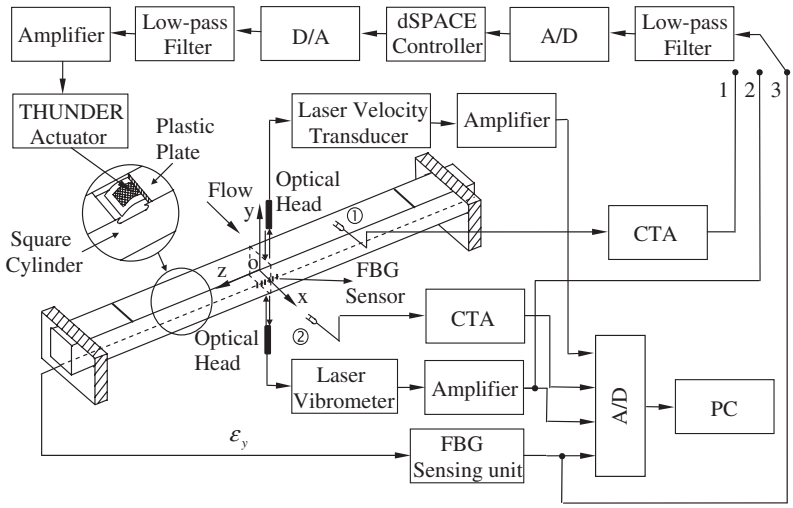

Fig. 1. Experimental setup. ① Feedback hot wire was located at $x/h = 0$, $y/h = 1.5$, $z/h = 5$; ② Monitor hot wire was located at $x/h = 2$, $y/h = 1.5$, $z = 0$.

free-stream velocity (U_∞) of 5.85 m/s, the cylinder underwent its first-mode resonance at the natural frequency $f_n = 47.9$ Hz of the structure, which was determined from the frequency response of the cylinder vibration when excited with an electromechanical shaker under no flow condition. Due to the light mass loading of the fluid, f_n was actually very close to the resonance frequency of the cylinder/fluid system, f_n'. The corresponding Re and the reduced velocity ($U_r = U_\infty/f_n'h$) were 6700 and 7.07. The maximum cylinder displacement, $Y_{\max}$, was about 0.91 mm or 0.05 h.

A 5 μm tungsten hot wire (hot wire ①) was placed at $x/h = 0$, $y/h = 1.5$ and $z/h = 5$ to measure the streamwise fluctuating velocity (u_1) of the flow. The cylinder vibration (Y) was measured using a laser vibrometer (Polytec OFV3100). Flexural deformation of the cylinder was monitored by a FBG sensor, buried in a groove located at the mid-span of the lower cylinder surface, to measure the dynamic strain ε_y of the cylinder associated with Y. The coordinates x, y and z correspond to streamwise, transverse and spanwise directions, as indicated in Fig. 1. The FBG sensor was holographically written on an optical silica fiber with a diameter of 125 μm and flushed with the surface using nail polish. Details of FBG sensing system and sensing principle were described in Jin et al. [21]. Since the sensor grating has a finite length of about 10 mm, the measurement represents an average strain over this spanwise length.

The above measured signals can be used as feedback signals either individually or in combination. After amplification, all feedback signals were low-pass filtered at a cut-off frequency of 200 Hz and then input into a Digital Signal Processor (DSP) fitted with 16-bit analog-to-digital (AD) and digital-to-analog (DA) converters. The converted analog signals were low-pass filtered again (cut-off frequency = 200 Hz) and amplified by two dual channel piezo-driver amplifiers (Trek PZD 700) before activating the actuators. The use of the two low-pass filters in the feed-forward and feedback passages was to remove high-frequency noises from turbulence and electronic components.

To monitor and analyze the control performance, a second 5 μm tungsten hot wire (hot wire ②) was placed at $x/h = 2$, $y/h = 1.5$, $z = 0$, where typical vortex-shedding signal was highly coherent. The measured fluctuating velocity (u_2) signal was amplified and recorded by a personal computer simultaneously with other sensors through a 12-bit AD board at a sampling frequency of 3.5 kHz per channel. The duration of each record was 20 s.

The LIF flow visualization and PIV measurements were conducted using a Dantec standard PIV2100 system, including a CCD camera for digital particle images and two New Wave standard pulsed laser sources for illumination. Each image covered an area of 176 mm × 141 mm or $x/h \approx 0.5$–10.8 and $y/h \approx -4.1$–4.1 of the flow field for both LIF flow visualization and PIV measurements. In addition, the cross-flow distributions of flow velocities and Reynolds stresses at $x/h = 3$ were measured using a two-component LDA system (Dantec Model 58N40 with an enhanced Flow Velocity Analyzer signal processor).

3. Controller design and parameter optimization

Based on the feedback signals, i.e. u_1, ε_y and Y, five different control schemes were investigated, which are divided into two categories. One is called one-element control scheme using a single signal from either flow field or cylinder vibration, referred to as u_Control, ε_y_Control and Y_Control, respectively. The other category is called two-element control scheme, which uses a

combination of two signals from both cylinder vibration and flow, namely, $u+\varepsilon_y$_Control and $u+Y$_Control.

For each control scheme, a feedback controller similar to the one used in Zhang et al. [22] was used, which applied a gain coefficient in amplitude ($\tilde{P}_q$) and a time shift ($\tilde{t}_q$) to the feedback signal q, representing u_1, ε_y or Y, to activate the actuators. The perturbation signal therefore contained various frequency components. Both $\tilde{P}_q$ and $\tilde{t}_q$ were manually tuned during experiments to ensure a maximum reduction in the root mean square (rms) value of Y, i.e. Y_{rms}, as detailed in following. For the one-element scheme, first vary $\tilde{P}_q$ by keeping $\tilde{t}_q = 0$ s to find a $\tilde{P}_q$, i.e. $\tilde{P}_{q,\mathrm{opt}}$, which leads to the smallest Y_{rms}. Then given $\tilde{P}_{q,\mathrm{opt}}$ vary $\tilde{t}_q$ within a range from 0 to 0.02 s to determine $\tilde{t}_{q,\mathrm{opt}}$, under which Y_{rms} reaches the minimum. The reason for choosing the duration of 0.02 s is the dominance of the first-mode resonance at f_n' (= 47.9 Hz ≈ the vortex-shedding frequency f_s) in the structural response. Therefore, the optimum $\tilde{t}_q$ is determined, which covers one complete cycle of the first mode oscillation, i.e. $1/f_n'$ (≈0.02 s). Then, the whole process is repeated on the basis of this optimum $\tilde{t}_q$ to arrive at the final optimal combination of $\tilde{P}_{q,\mathrm{opt}}$ and $\tilde{t}_{q,\mathrm{opt}}$. For the two-element scheme, the same tuning process as the one-element scheme was first carried out for each feedback signal to obtain an initial configuration. Then apply simultaneously the two signals selected using the initial configuration as a starting point for fine tuning, in which both $\tilde{P}_q$ and $\tilde{t}_q$ were adjusted again for each signal. Several iterations were needed to reach the final configuration, giving the maximum reduction in Y_{rms}.

The whole controller design process was carried out using a digital open source platform dSPACE. This platform provided a real-time system for rapid control prototyping, production code generation, and hardware-in-the-loop tests. A digital signal processor (DSP) with SIMULINK function of MATLAB and software (ControlDesk 2.0) was used for sampling and processing feedback signals.

Fig. 2 shows two typical examples of parameter tuning for u_Control (Fig. 2(a)) and $u+Y$_Control (Fig. 2(b)). The rms value of u_2 ($u_{2,\mathrm{rms}}$), normalized by U_∞, and ε_y ($\varepsilon_{y,\mathrm{rms}}$) were simultaneously measured during tuning. Before control, the Y_{rms}/h, $\varepsilon_{y,\mathrm{rms}}$ and $u_{2,\mathrm{rms}}/U_\infty$ are 0.041, 297μ and 0.24, respectively. For u_Control (Fig. 2(a)), all three quantities exhibit a dip at $\tilde{P}_{u_1} = 2$ when $\tilde{t}_{u_1} = 0$ s (upper trace). Varying $\tilde{t}_{u_1}$ within a range from 0 to 0.02 s by keeping $\tilde{P}_{u_1} = 2$ further reduces their amplitude to a minimum at $\tilde{t}_{u_1} = 0.006$ s before they reach a local maximum at $\tilde{t}_{u_1} = 0.016$ s (lower trace). This time delay, i.e. $0.016 - 0.006$ s $= 0.01$ s, corresponds roughly to one-half of the period of the first-mode vibration f_n', suggesting an anti-phased relation between the two extreme cases. The $u+Y$_Control requires tuning two sets of parameters, ($\tilde{P}_{u_1}, \tilde{t}_{u_1}$) and ($\tilde{P}_Y, \tilde{t}_Y$). Fig. 2(b) shows the variation of the three physical quantities with respect to one set of parameter, while the other set is set to be optimal. It is clear that, when changing parameters in the controller, all three quantities undergo similar changes, pointing to the possibility to achieve a simultaneous control of both vortex shedding and the structural vibration using the same controller. The tuning process led to an optimal configuration for each scheme with parameters tabulated in Table 1. Unless otherwise stated, these parameters were used in experiments discussed hereinafter.

4. Control performance

Figs. 3–5 compare with the un-controlled case the control performances of the five control schemes in terms of the power spectra, E_Y, E_{ε_y} and E_{u_2}, of Y, ε_y and u_2. The spectrum of

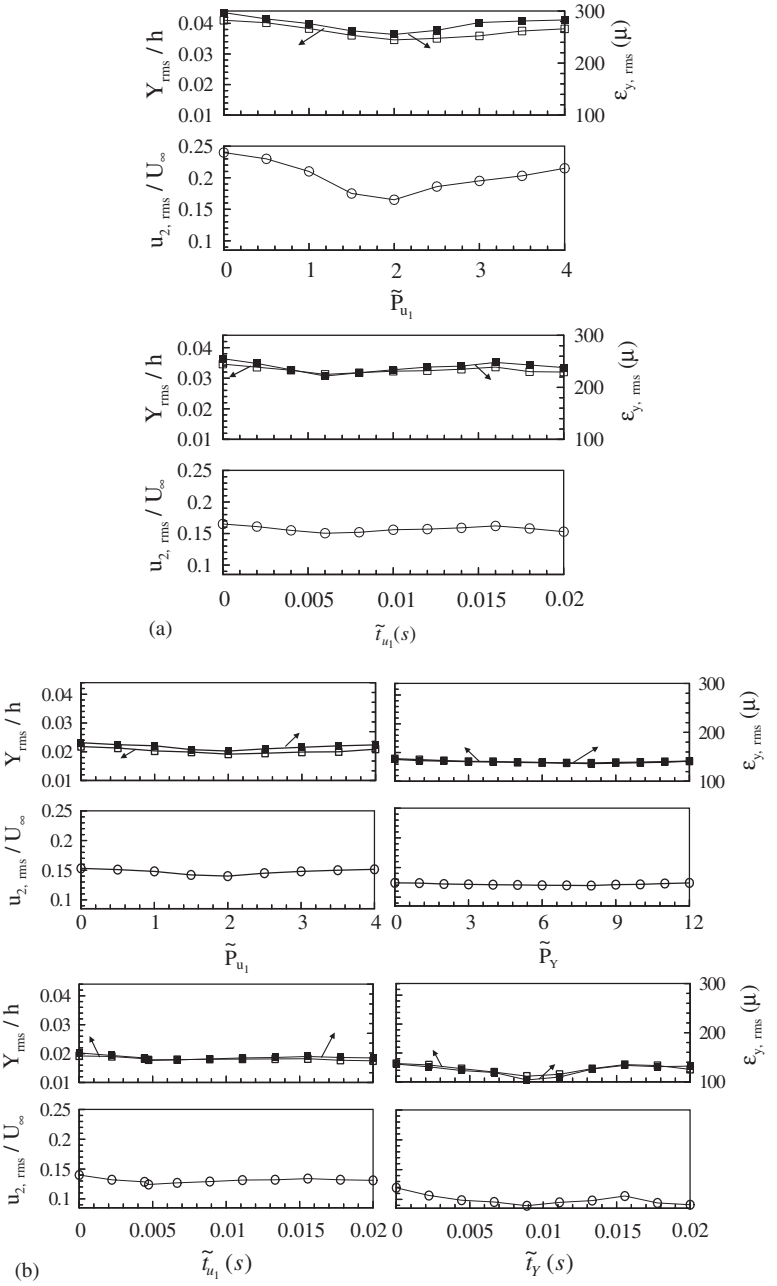

Fig. 2. Typical closed-loop control response of normalized rms. values of structural vibration (Y_{rms}), fluctuating streamwise flow velocity ($u_{2,\mathrm{rms}}$), fluctuating strain in y-direction, $\varepsilon_{y,\mathrm{rms}}$ under different control schemes: (a) u_Control and (b) $u+Y$_Control. $Re = 6700$. $U_r = 7.07$. Y_{rms}/h; $\varepsilon_{y,\mathrm{rms}}$; $u_{2,\mathrm{rms}}/U_\infty$.

Table 1
Optimal $\tilde{P}_q$ and $\tilde{t}_q$ (q represents $u1, \varepsilon_y$ or Y) under different control schemes

Optimal parameter	Control scheme				
	u_Control	ε_y_Control	Y_Control	$u+\varepsilon_y$_Control	$u+Y$_Control
$\tilde{P}_{u_1}$	2			0.4	2
$\tilde{t}_{u_1}$	0.0060 s			0.0067 s	0.0047 s
$\tilde{P}_{\varepsilon_y}$		6		6	
$\tilde{t}_{\varepsilon_y}$		0.0040 s		0.0072 s	
$\tilde{P}_Y$			10		8
$\tilde{t}_Y$			0.0080 s		0.0089 s

fluctuation α, representing Y, ε_y or u_2, has been normalized, such that $\int_0^\infty E_\alpha(f)\,\mathrm{d}f = 1$. The frequency f was normalized with h and U_∞ in this paper ($f^* = fh/U_\infty$). The effects of different control schemes on the cylinder vibration are illustrated by Figs. 3 and 4. Three pronounced peaks appear in the spectra at different frequencies. The first peak corresponds to the first-mode natural frequency, $f_n'^*$, of the fluid–structure system, which coincides with the shedding frequency f_s^* ($f_n'^* = f_s^* = 0.141$). The second one at $2f_s^*$ is the second harmonic of f_s^* and the third one at $f_n'''^* = 0.49$ is the third-mode natural frequency of the system. Given the second-mode vibration anti-symmetrical about the mid-span of the cylinder, no peak is expected at the second-mode natural frequency of the system. When the one-element control is deployed (Figs. 3 and 4(b)–(d)), there is a systematic reduction in both E_Y and E_{ε_y} compared to their un-controlled counterparts. Y_Control is best performed to suppress the resonant peaks at $f_n'^*$ and $f_n'''^*$, which drop from 0.21 and 0.13 to 0.096 and 0.066 at $f_n'^*$ in E_Y and E_{ε_y}, respectively, and from 0.14 and 0.06 to 0.016 and 0.019 at $f_n'''^*$, respectively. Note that u_Control may perform better in suppressing the peak at $2f_s^*$ in E_Y than Y_Control (Fig. 3(b)). This is reasonable since structural vibration at $2f_s^*$ is mainly due to the second harmonic of the shedding frequency. The use of fluid sensor therefore brings more relevant information on flow into the controller. The two-element control schemes in general improve the control performance of the one-element scheme (Figs. 3 and 4(e)–(f)). The best result is achieved using $u+Y$_Control, with the peak amplitude at $f_n'^*$ reduced by 79% and 68% or by 94% and 75% at $f_n'''^*$ in E_Y and E_{ε_y}, respectively.

Fig. 5 shows the corresponding u_2-spectrum. In the un-perturbed case, E_{u_2} displays three harmonics of the shedding frequency. The peak at $3f_s^*$ is completely eliminated for all five control schemes, while those at f_s^* and $2f_s^*$ are suppressed to different degrees. Among the three one-element control schemes, u_Control is best performed due to the direct feedback from the flow. Again, the two-element control schemes outperform the one-element control schemes in suppressing these peaks.

Fig. 6 presents the reduction, compared with the unperturbed case, in energies in E_Y and E_{ε_y} associated with the vibration of different peaks, i.e. $E^{(m)}_{Y,\Delta f}$ and $E^{(m)}_{\varepsilon_y,\Delta f}$ ($m = 1, 2, 3$), or in energies in E_{u_2} associated with the harmonics of f_s^*, i.e. $E^{(n)}_{u_2,\Delta f}$ ($n = 1, 2, 3$). These energies were calculated by integrating the power spectral density functions over -3 dB bandwidth centered about each peak. As it is evident in Fig. 6(a) and (b), the two-element schemes obviously perform better than the

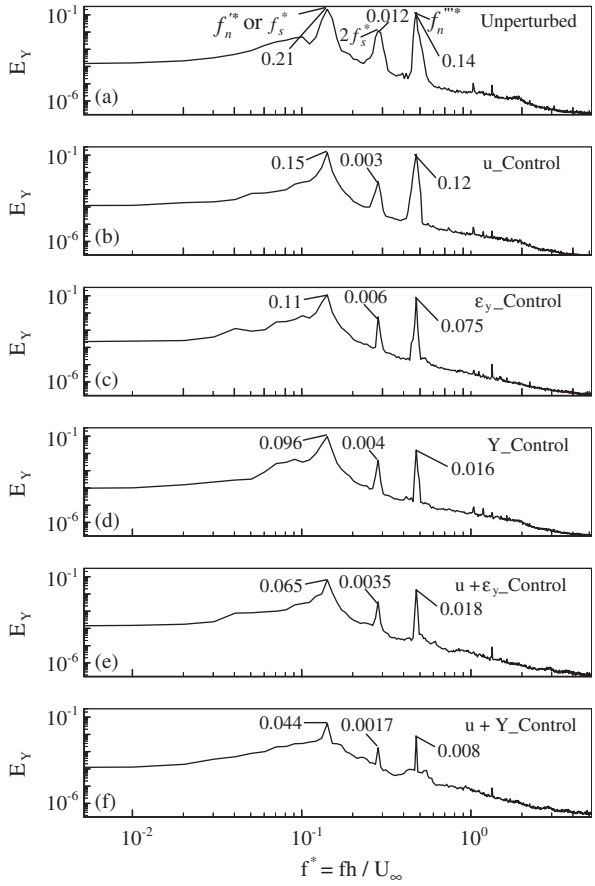

Fig. 3. Effect on power spectrum of structural vibration (Y), E_Y, under different control schemes: (a) unperturbed; (b) u_Control; (c) ε_y_Control; (d) Y_Control; (e) $u+\varepsilon_y$_Control and (f) $u+Y$_Control. $Re = 6700$. $U_r = 7.07$.

one-element schemes in terms of suppressing structural vibration, especially the first-mode resonance. In the best case, $u+Y$_Control reduces $E^{(1)}_{Y,\Delta f}$, $E^{(2)}_{Y,\Delta f}$ and $E^{(3)}_{Y,\Delta f}$ by 81.5%, 85.2% and 98.2%, and $E^{(1)}_{\varepsilon_y,\Delta f}$, $E^{(2)}_{\varepsilon_y,\Delta f}$ and $E^{(3)}_{\varepsilon_y,\Delta f}$ by 77.4%, 79.5% and 96.2%, respectively. On the other hand, u_Control (Fig. 6(c)) greatly impairs vortex shedding, and the performance is further improved if the feedback consists of a combination of u and Y (or ε_y). The best performance is given by $u+Y$_Control, which reduces $E^{(1)}_{u_2,\Delta f}$, $E^{(2)}_{u_2,\Delta f}$ and $E^{(3)}_{u_2,\Delta f}$ by 80.3%, 86.5% and 96.4%, respectively. It is interesting to note that all control schemes are effective to suppress not only the vibration of the first-mode but also, even to a larger extent, that of the third-mode.

Figs. 7–9 show the typical time histories of Y, ε_y and u_2 under Y_Control and $u+Y$_Control, respectively. Under $u+Y$_Control, the amplitudes of u_2, ε_y, Y are reduced drastically in all cases. A comparison of all five schemes in time domain (not shown) indicates that the effectiveness of the schemes is improved following the ladder of u_, ε_y_, Y_, $u+\varepsilon_y$_ and $u+Y$_Control. Interestingly, the control voltage and the perturbation amplitude required by each scheme are gradually

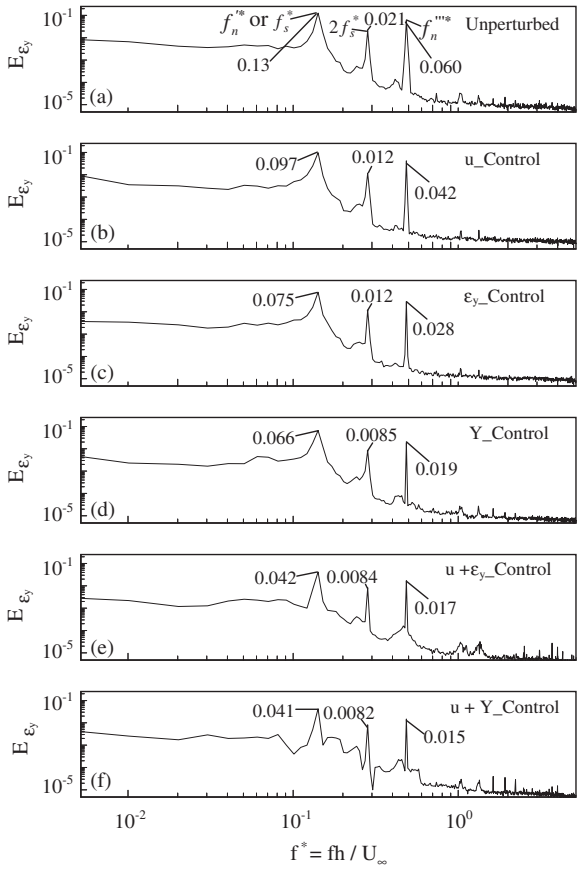

Fig. 4. Effect on power spectrum of fluctuating strain in y direction (ε_y), E_{ε_y}, under different control schemes: (a) unperturbed; (b) u_Control; (c) ε_y_Control; (d) Y_Control; (e) u+ε_y_Control and (f) $u+Y$_Control. $Re = 6700$. $U_r = 7.07$.

decreased following the same order, as indicated by the rms value, $V_{p,\mathrm{rms}}$, of the control voltage and the ratio (Table 2), $Y_{p,\mathrm{rms}}/Y_{\mathrm{rms}}$, of the perturbation displacement to that of the cylinder in the absence of perturbation. Here $Y_{p,\mathrm{rms}}$ was obtained based on the measurement of two laser vibrometers, pointing at the centre of the plastic plate and that of the cylinder, respectively (Fig. 1). Since the resistance of the actuators remains constant irrespective of the control schemes, a lower control voltage means a lower energy input. Evidently, $u+Y$_Control requires the lowest actuating voltage and the smallest perturbation displacement (roughly 20% of the unperturbed structural displacement) than other four schemes yet achieves the best performance of all (71% reduction in Y_{rms}, 65% in $\varepsilon_{y,\mathrm{rms}}$ and 63% in $u_{2,\mathrm{rms}}$).

5. Discussions

To understand the physics behind the impaired Y and ε_y, the modified flow structure under the control schemes measured by LIF flow visualization, PIV and LDA measurements were

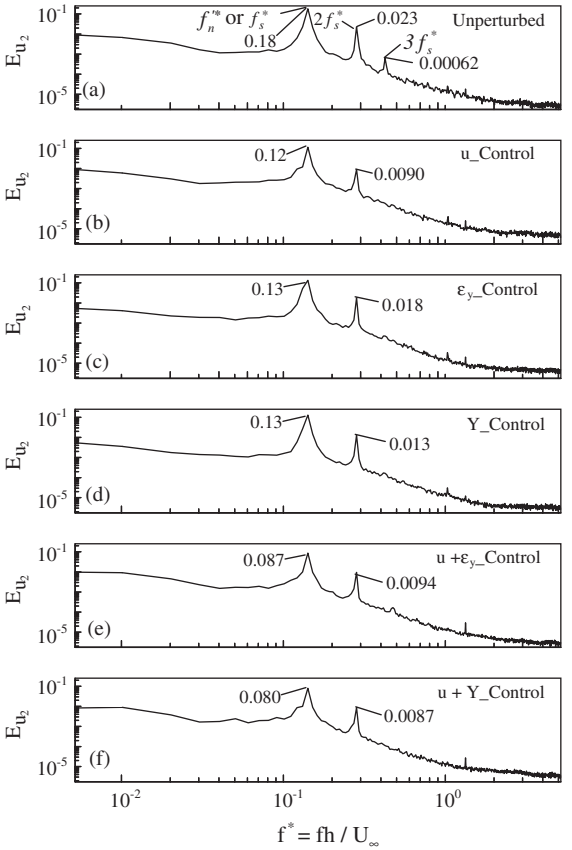

Fig. 5. Effect on power spectrum of streamwise flow velocity (u_2), E_{u_2}, under different control schemes: (a) unperturbed; (b) u_Control; (c) ε_y_Control; (d) Y_Control; (e) $u+\varepsilon_y$_Control and (f) $u+Y$_Control. $Re = 6700$. $U_r = 7.07$.

first examined. Without control, the Kármán vortex street is evident in Figs. 10(a) and 11(a). The solid square in the figures corresponds to the cylinder position. Once a control scheme is deployed, vortex shedding from the cylinder and the normalized maximum spanwise vorticity, $|\omega_{z\,\max}^*| = |\omega_{z\max}|h/U_\infty$, are weakened to various degrees, depending on the schemes used, as evident in Figs. 10(b)–(f) and 11(b)–(f); vortices appear breaking up, showing considerably less coherence and weaker strength. The most significant alteration to the flow is obtained when the two two-element control schemes are applied (Figs. 10(e)–(f) and 11(e)–(f)). For $u+Y$_Control scheme, the vortex street is almost completely destroyed; the corresponding $|\omega_{z\,\max}^*|$ and circulation (Γ) decreases by 60% and 85%. Γ around a vortex is estimated by numerical integration $\Gamma^* = (\Gamma/U_\infty h) = \sum_{i,j}(\omega_z^*)_{ij}(\Delta A/h^2)$ [23], where $\left(\omega_z^*\right)_{ij}$ is spanwise vorticity over area $\Delta A = \Delta x \Delta y$, Δx and Δy being the integral step along x- and y-directions, respectively. Integration was conducted over an area enclosed by the cut-off level $|\omega_{zc}^*| = 0.3$, about 6% of $|\omega_{z\,\max}^*|$, which is the same as Cantwell and Coles [23].

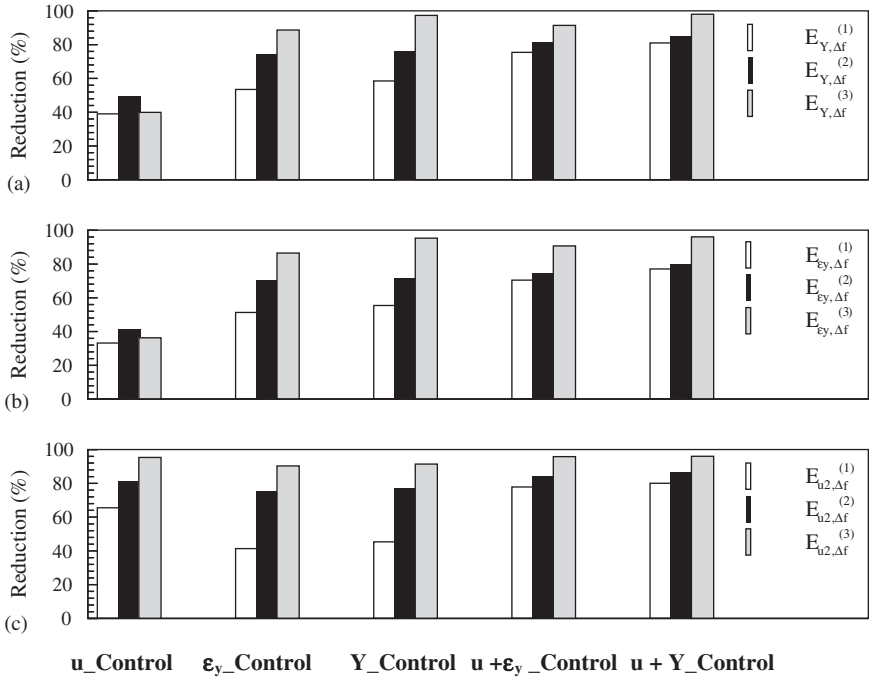

Fig. 6. Reduction in $E_{Y,\Delta f}^{(m)}$, $E_{\varepsilon_y,\Delta f}^{(m)}$ and $E_{u_2,\Delta f}^{(n)}$ ($m, n = 1, 2, 3$). (a) Y, (b) ε_y and (c) u_2. $Re = 6700$. $U_r = 7.07$.

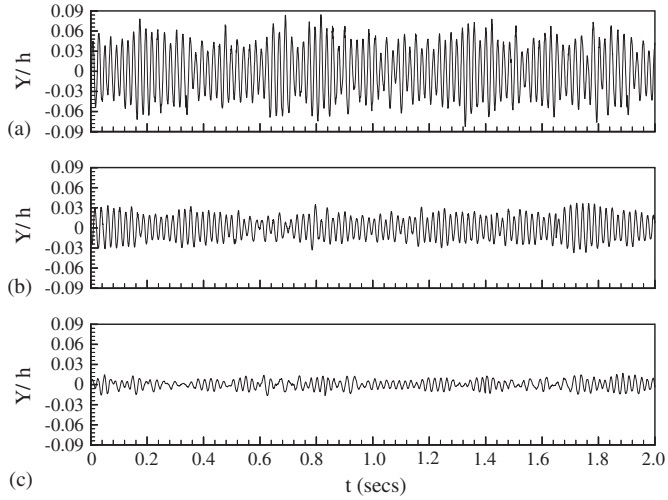

Fig. 7. Typical time histories of structural vibration (Y) under different control schemes: (a) unperturbed; (b) u_Control; (c) ε_y_Control; (d) Y_Control; (e) $u+\varepsilon_y$_Control and (f) $u+Y$_Control. $Re = 6700$. $U_r = 7.07$. The time origin was arbitrary.

Fig. 12 exhibits the modification of the cross-flow distributions of the mean velocity $\overline{U}^*$, normalized by U_∞, and Reynolds stresses $\overline{u^2}^*$, $\overline{v^2}^*$ and $\overline{uv}^*$, normalized by U_∞^2, measured by LDA at $x/h = 3$ under the $u+Y$_Control scheme. In the range of $y/h = -1.4$ to 1.4, the maximum $\overline{U}^*$,

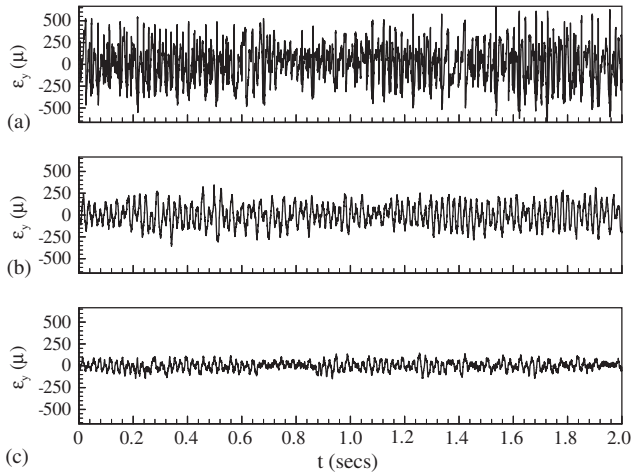

Fig. 8. Typical time histories of fluctuating strain in the y-direction (ε_y) under different control schemes: (a) unperturbed; (b) u_Control; (c) ε_y_Control; (d) Y_Control; (e) $u+\varepsilon_y$_Control and (f) $u+Y$_Control. $Re = 6700$. $U_r = 7.07$. The time origin was arbitrary.

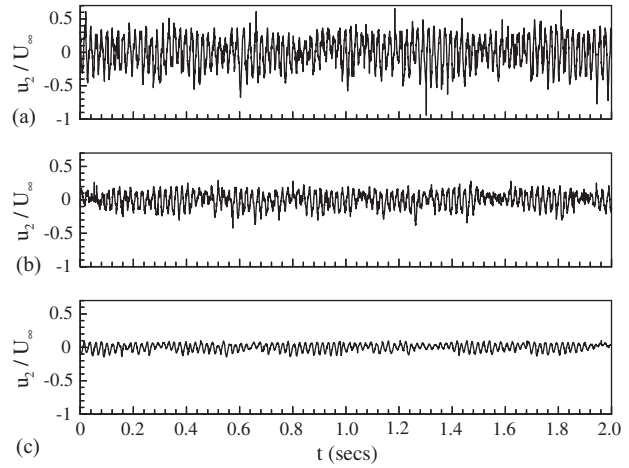

Fig. 9. Typical time histories of streamwise flow velocity (u_2) under different control schemes: (a) unperturbed; (b) u_Control; (c) ε_y_Control; (d) Y_Control; (e) $u+\varepsilon_y$_Control and (f) $u+Y$_Control. $Re = 6700$. $U_r = 7.07$. The time origin was arbitrary.

Table 2
Control voltage and the perturbation/structural displacement ratio in the five control schemes

	Control scheme				
	u_Control	ε_y_Control	Y_Control	$u+\varepsilon_y$_Control	$u+Y$_Control
$V_{p,\mathrm{rms}}$ (V)	106	94	80	62	54
$Y_{p,\mathrm{rms}}/Y_{\mathrm{rms}}$ (%)	42	32	28	22	20

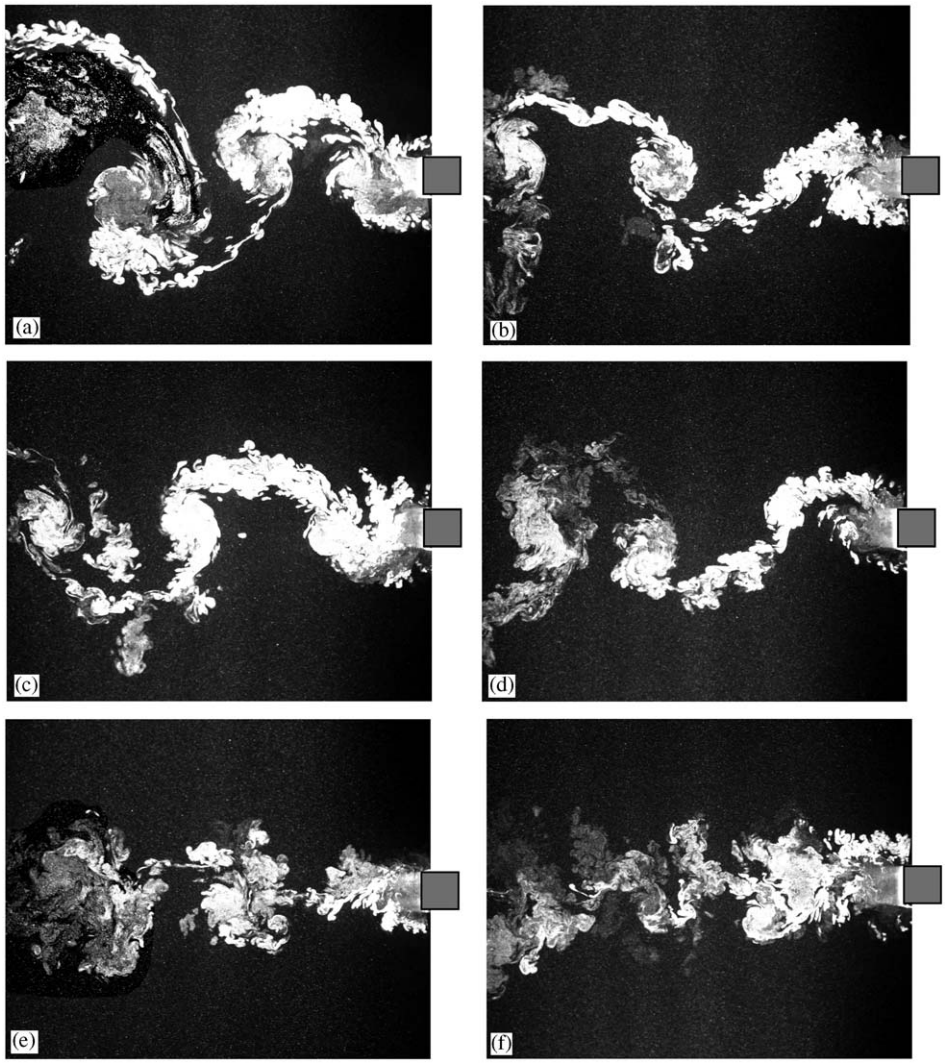

Fig. 10. Typical photographs from LIF flow visualization under different control schemes: (a) unperturbed; (b) u_Control; (c) ε_y_Control; (d) Y_Control; (e) $u+\varepsilon_y$_Control and (f) $u+Y$_Control. $Re = 6700$. $U_r = 7.07$.

$\overline{u^2}^*$ and $\overline{v^2}^*$ decline considerably, up to 14%, 19%, 19%, respectively, compared with those unperturbed. On the other hand, $\overline{uv}^*$ increases by about 21%. The increased mean velocity deficit is related to the decreased entrainment of high speed fluid from the free-stream under the action of the weakened vortices [9]. Evidently, the weakened vortices are responsible for the decrease in $\overline{u^2}^*$ and $\overline{v^2}^*$, and accordingly the increased $\overline{uv}^*$ since $\overline{uv}^*$ is largely associated with the incoherent motion, residing in the saddle region between two consecutive vortices [24]. Note that $\overline{U}^*$, $\overline{u^2}^*$ and $\overline{v^2}^*$ remain reasonably symmetric and $\overline{uv}^*$ is anti-symmetric about the centerline although the perturbation was imposed only on the upper side of the cylinder, in line with the flow patterns shown in Figs. 10 and 11.

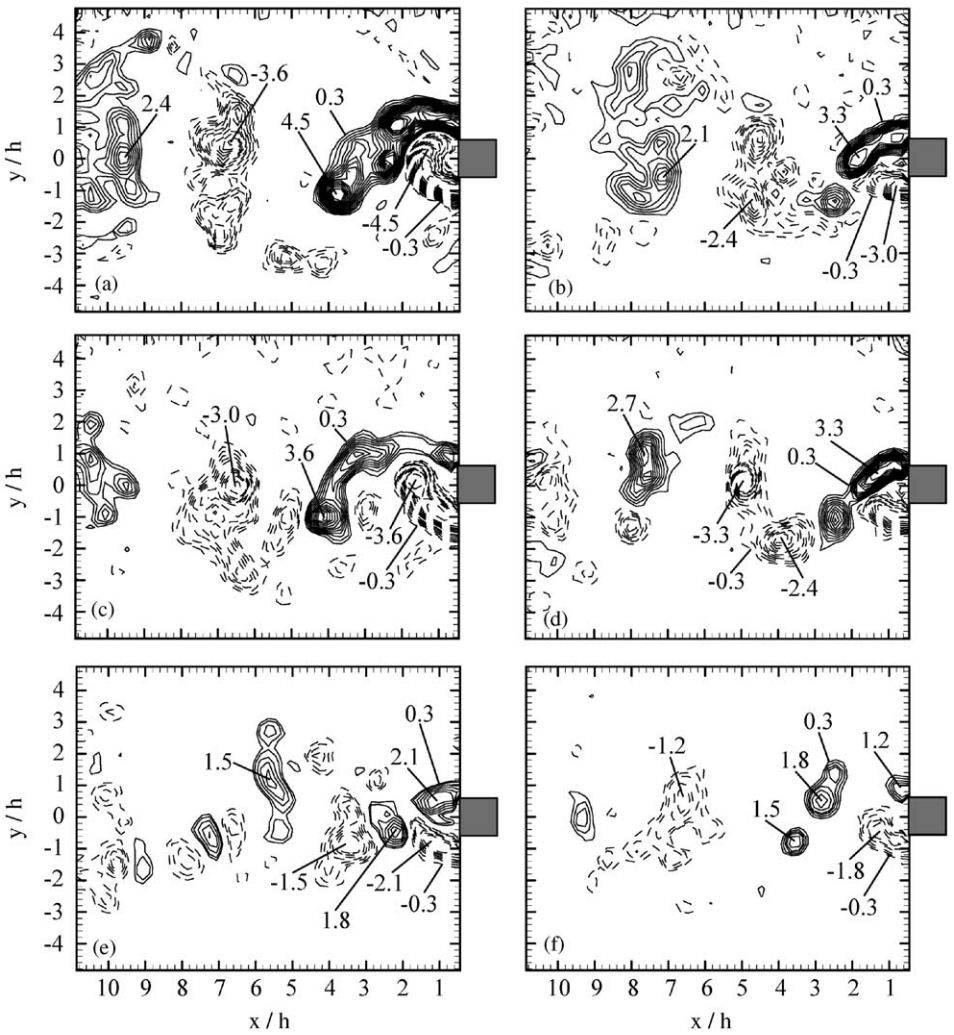

Fig. 11. PIV measured iso-contours of spanwise vorticity $\omega_z^* = \omega_z h/U_\infty$ under different control schemes: (a) unperturbed; (b) u_Control; (c) ε_y_Control; (d) Y_Control; (e) $u+\varepsilon_y$_Control and (f) $u+Y$_Control. $Re = 6700$. $U_r = 7.07$.

The mean drag coefficient, $\overline{C}_D$, was calculated based on $\overline{U}^*$, $\overline{u^2}^*$ and $\overline{v^2}^*$ [25]

$$\overline{C}_D = 2\int_{-\infty}^{\infty} \frac{\overline{U}}{U_\infty}\left(\frac{U_\infty - \overline{U}}{U_\infty}\right) d\left(\frac{y}{h}\right) 2\int_{-\infty}^{\infty}\left(\frac{\overline{v^2}+\overline{u^2}}{U_\infty^2}\right) d\left(\frac{y}{h}\right). \tag{1}$$

$\overline{C}_D$ was 2.09 for the uncontrolled case, agreeable with the previously reported range, 1.7–2.2 [26–28]. Under $u+Y$_Control scheme, $\overline{C}_D$ dropped by 30%. Apparently, the weakened vortex shedding should correspond to an increased backpressure and subsequently reduced $\overline{C}_D$.

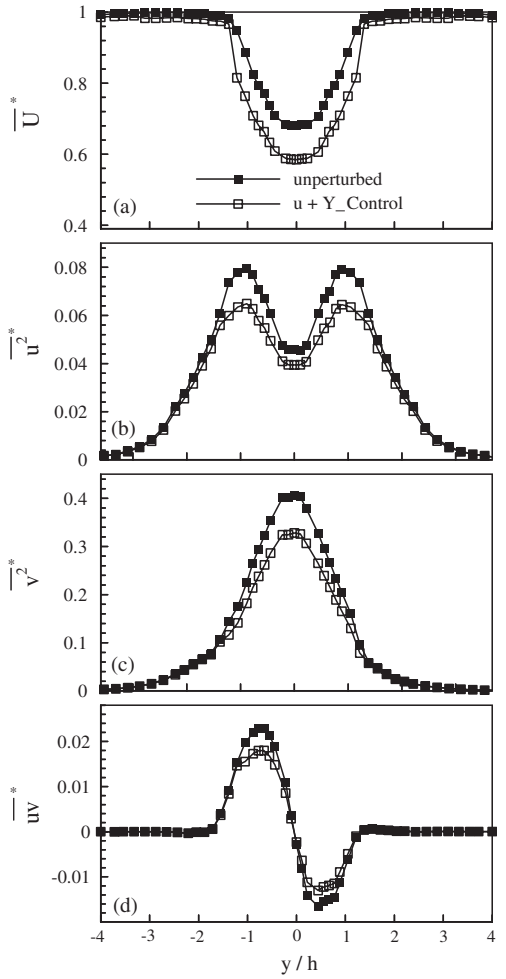

Fig. 12. Cross-flow distribution of mean velocity and Reynolds stresses at $x/h = 3$ with and without control: (a) $\overline{u^2}^*$, (b) $\overline{u^2}^*$, (c) $\overline{v^2}^*$ and (d) $\overline{uv}^*$. $U_r = 7.07$.

Insight into the physics behind the modified flow and structural vibration may be better gained by examining the spectral phase and coherence between the simultaneously measured Y and u_2, i.e. $\phi_{Yu_2} \equiv \tan^{-1}(Q_{Yu_2}/\mathrm{Co}_{Yu_2})$ and $\mathrm{Coh}_{Yu_2} = (\mathrm{Co}^2_{Yu_2} + Q^2_{Yu_2})/E_Y E_{u_2}$, where Co_{Yu_2} and Q_{Yu_2} stand for the cospectrum and quadrature spectrum of Y and u_2, respectively. Coh_{Yu_2} provides a measure of the degree of correlation between the Fourier components of Y and u_2. The cross-spectrum was computed using the fast Fourier transform (FFT) method [29]. Cheng et al. [16] demonstrated that ϕ_{Yu_2} was approximately equivalent to the phase relationship between the lateral structural oscillating velocity, $\dot{Y}$, and the lateral velocity, v, of the flow around the cylinder. Hence, $\phi_{Yu_2} = 0$ and $-\pi$ indicate the synchronized and opposite movements between $\dot{Y}$ and v, respectively. Without perturbation, ϕ_{Yu_2} was about zero near $f_s^* = f_n'^*$, $2f_s^*$ and $f_n'''^*$ (Fig. 13(a)), that is, $\dot{Y}$ and v were synchronized at these frequencies. The plateaus around f_s^* (or $f_n'^*$), $2f_s^*$ and $f_n'''^*$ indicated that

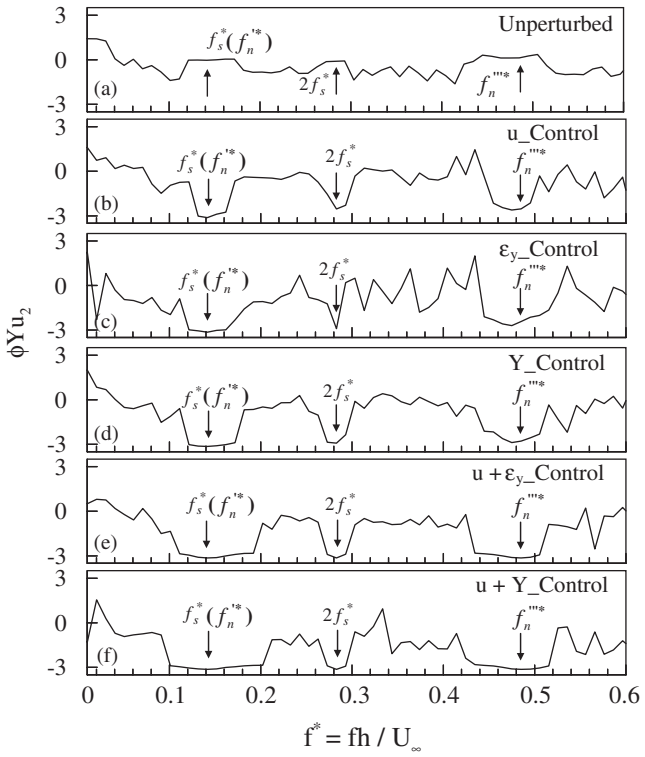

Fig. 13. Phase shift ϕ_{Yu_2} between structural vibration (Y) and fluctuating streamwise flow velocity (u_2) under different control schemes. $Re = 6700$. $U_r = 7.07$.

the synchronization occurred over a range of frequencies. However, ϕ_{Yu_2} at these frequencies was changed from 0 to near $-\pi$ under different control schemes (Figs. 13(b)–(f)), suggesting that $\dot{Y}$ and v collided or acted against each other, resulting in impaired vortex shedding and cylinder vibration. This phase change was most extensive under the two-element schemes for $f_n'^*$, $2f_s^*$ and $f_n'''^*$, explaining its superior performance over the one-element schemes. Accordingly, Coh_{Yu_2} at f_2^* (or $f_n'^*$), $2f_s^*$ and $f_n'''^*$, receded greatly (Fig. 14); for $u+Y$_Control (Fig. 14(f)), it reduced by 74.2%, 67.0% and 83.2%, respectively, around the three frequencies, compared with the unperturbed case. The drastic reduction in Coh_{Yu_2} implied a nearly decoupled correlation between vortex shedding and structural vibration.

From a different perspective, the alteration in ϕ_{Yu_2} and reduction in Coh_{Yu_2} can be related to an altered fluid–structure system damping. Damping simulates the energy dissipation of a dynamic system during vibrations and plays an important role in any resonant system. The effective damping used here is defined as the sum of structural damping and fluid damping. The former may be generated by material, friction, impacting and rubbing of two surfaces in contact, while the latter results from skin friction and viscous dissipation, i.e. viscous shearing of a fluid at the surface of the structure and flow separation [1]. The free vibration of a flexible structure consists of multiple modal oscillations and each of them corresponds to a different effective damping ratio.

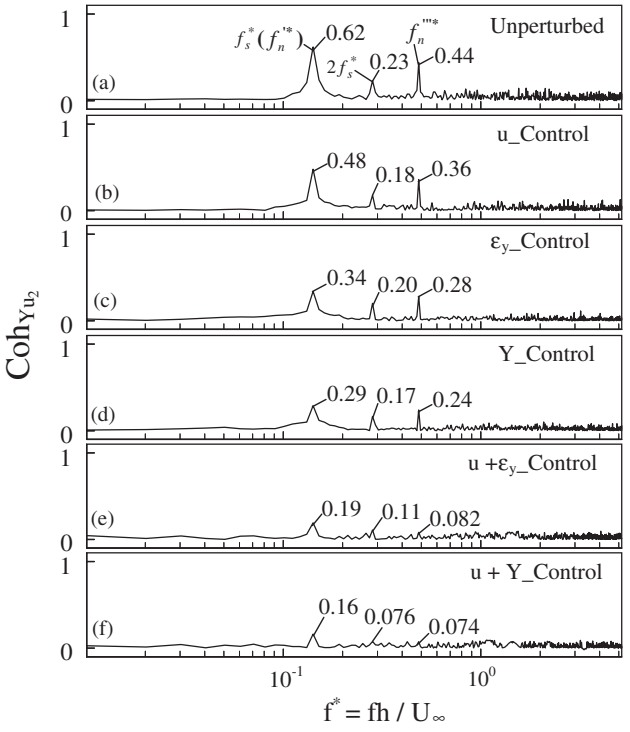

Fig. 14. Spectra coherence (Coh_{Yu_2}) between structural vibration (Y) and fluctuating streamwise flow velocity (u_2) under different control schemes. $Re = 6700$. $U_r = 7.07$.

An auto-regressive moving average (ARMA) technique was used to calculate the effective damping ratios, associated with $f_n'^*$ and $f_n'''^*$, i.e. $\zeta_{y,e}^{(k)}$ ($k = 1, 3$), from the measured time-domain Y signals. Details about ARMA technique can be found in Zhou et al. [30]. The ARMA model of an order of 190 and 70 000 data points was presently used for calculation. Fig. 15 shows the effective first- and third-mode damping ratios for different schemes. The corresponding structural damping ratios, $\zeta_{y,s}^{(k)}$, indicated by a dash line, were measured in air under no-flow condition with the cylinder excited by an electromechanical shaker. Without control, vortex shedding synchronized with the lateral structural vibration, and $\zeta_{y,e}^{(k)}$ was less than $\zeta_{y,s}^{(k)}$, albeit slightly, suggesting a negative fluid damping ratio $\zeta_{y,f}^{(k)}$ since $\zeta_{y,e}^{(k)} = \zeta_{y,s}^{(k)} + \zeta_{y,f}^{(k)}$. The negative $\zeta_{y,f}^{(k)}$ simply means that vortex shedding enhances the structural vibration [30]. $\zeta_{y,e}^{(k)}$ increased gradually following the ladder of $u\_$, $\varepsilon_y\_$, $Y\_$, $u + \varepsilon_y\_$ and $u + Y_$Control. The maximum damping ratio was obtained under $u + Y_$Control, in which $\zeta_{y,e}^{(1)}$ and $\zeta_{y,e}^{(3)}$ rose by 60% and 87%, respectively, compared with uncontrolled case. The variation in $\zeta_{y,e}^{(1)}$ and $\zeta_{y,e}^{(3)}$ was agreeable with the trend shown in Figs. 2–4 and 6–8, providing an explanation for the effectively attenuated structural oscillations.

An interpretation of the closed-loop control mechanism is now proposed. Structural vibration of a bluff body in a cross-flow originates from fluid-excitation forces due to the vortex shedding.

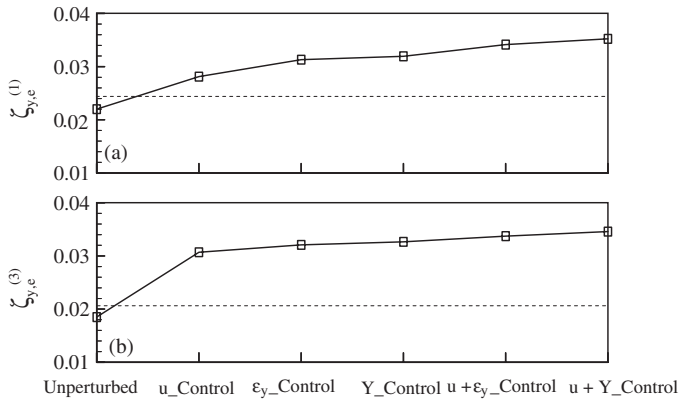

Fig. 15. Effect of closed-loop control on the effective damping ratios associated the first and third modal oscillation frequencies: (a) $\zeta_{y,e}^{(1)}$ and (b) $\zeta_{y,e}^{(3)}$. The dash line denotes the structural damping ratio $\zeta_{y,s}^{(k)}$ measured without flow. $Re = 6700$. $U_r = 7.07$.

The resultant structural vibrations in turn influence the flow field, giving rise to fluid–structure coupling. Fluid excitations with a high-energy concentration at f_s^* and $2f_s^*$ cause structure resonance at $f_n'^*$ and strong oscillations at $f_n'''^*$. At these frequencies, the structural vibration is in-phase with the vortex shedding. The control effect successfully alters the nature of the fluid–structure interactions, changing the in-phased fluid–structure synchronization into anti-phased interactions. This leads to an effective impairment of vortex shedding and a simultaneous enhancement of fluid–structure damping. As a result, the structural vibration is attenuated.

The one-element control schemes use either flow or structural response as feedback. The flow response u_2 contains only information on the flow excitation and nothing on the structural vibration. Thus, u_Control alters the flow excitation and therefore indirectly affects the structural vibration. On the other hand, both ε_y_ and Y_Control schemes use the structural vibration information, without the flow, for feedback, performing better in suppressing the vibration than u_Control scheme. Note that ε_y is a measure of the structural deformation, which indirectly reflects the vibration, while Y is a direct measure of the lateral structural movement, which is the direct agent to communicate with flow. Consequently, Y_Control performs better than ε_y_Control (Figs. 3–6 and 10 and 11). Since the one-element schemes use signals from either flow or structural vibration, the information on the nonlinear flow–structure interaction is not made use of. This information is, however, an important part of physics behind the vortex-induced vibrations. Therefore, the schemes cannot achieve the best performance. On the other hand, the two-element schemes utilize a combination of flow and structural vibration signals for feedback and reflect the interaction/coupling between flow and structural vibration, addressing the essence that governs both structural vibration and vortex shedding. As a result, the two-element schemes outperform the one-element scheme, even though the input energies to the actuators are appreciably lower. For the two two-element schemes, the better performance of $u + Y$_Control is due to the direct relationship of Y with the structural vibration, on the one hand, and the direct interaction of Y with flow, on the other hand.

6. Conclusions

Experimental investigation has been conducted to control the vortex-induced resonant vibration of a fix-supported flexible cylinder based on various feedback signals. The control was made possible by perturbing one surface of the cylinder using piezoceramic actuators embedded underneath the structure surface. Five control schemes are investigated depending on the feedback signal used. The three one-element schemes, namely $u\_$, $\varepsilon_y\_$ and $Y_$Control, deploy feedback signal either from flow or from cylinder vibration. The two-element control schemes, namely $u+\varepsilon_y\_$ and $u+Y_$Control, use a combination of both structural vibration and flow signals. The investigation leads to the following conclusions.

1. The resonant flexural vibration of a flexible cylinder in a cross-flow can be successfully controlled using the present perturbation technique. Under the control, the phase relationship between vortex shedding and structural displacement at $f_s^*(f_n'^*)$, $2f_s^*$ and $f_n'''^*$ is changed from in-phase to anti-phase. This alters the synchronized motion between fluid and structure to collision between them, causing significantly increased modal damping ratios of the fluid–structure system. Consequently, vortex shedding is impeded and the structural vibration is effectively reduced.
2. A suitable choice of the feedback signal is crucial in determining the effectiveness of the control. The control performances in terms of suppressing structural vibration are gradually improved following the ladder of $u\_$, $\varepsilon_y\ \_$, $Y\_$, $u+\varepsilon_y\_$ and $u+Y_$Control. The two-element schemes perform much better than the one-element scheme, in terms of suppressing both vortex shedding and structural vibration. Furthermore, the input energy required by the two-element schemes is minimum. The results are ascribed to its feedback signals, which reflect the interactions between fluid and structure. Among all schemes, $u+Y_$Control performs best, resulting in a reduction by 71% in Y, 65% in ε_y, 63% in u_2, 85% in Γ and 30% in $\overline{C}_D$, compared with their uncontrolled counterparts.

Acknowledgments

The authors wish to acknowledge support given to them by a grant from Research Grants Council of Hong Kong Special Administrative Region, China (Project No. PolyU 5294/03E). L. Cheng wishes to acknowledge the support from a special fund for new Chair Professors given by The Hong Kong polytechnic University.

References

[1] R.D. Blevins, *Flow-Induced Vibration*, second ed., Krieger Publishing Company, Malabar, FL, 1994.
[2] M.S. Howe, *Acoustics of Fluid–structure Interactions*, Cambridge University Press, UK, 1998.
[3] M. Gad-el-Hak, Flow control: the future, *Journal of Aircraft* 38 (2001) 402–418.
[4] M.M. Zdravkovich, Review and classification of various aerodynamic and hydrodynamic means for suppressing vortex shedding, *Journal of Wind Engineering and Industrial Aerodynamics* 7 (1981) 145–189.

[5] M.J. Every, R. King, D.S. Weaver, Vortex-excited vibrations of cylinders and cables and their suppression, *Ocean Engineering* 9 (1982) 135–157.
[6] J.F. Wilson, J.C. Tinsley, Vortex load reduction: experiments in optimal helical strake geometry for rigid cylinders, *ASME Journal of Energy Resources Technology* 111 (1989) 72–76.
[7] F.B. Hsiao, J.Y. Shyu, Influence of internal acoustic excitation upon flow passing a circular cylinder, *Journal of Fluids and Structures* 5 (1991) 427–442.
[8] D.R. Williams, H. Mansy, C. Amato, The response and symmetry properties of a cylinder wake subjected to localized surface excitation, *Journal of Fluid Mechanics* 234 (1992) 71–96.
[9] H.M. Warui, N. Fujisawa, Feedback control of vortex shedding from a circular cylinder by cross-flow cylinder oscillations, *Experiments in Fluids* 21 (1996) 49–56.
[10] P.T. Tokumaru, P.E. Dimotakis, Rotary oscillation control of a cylinder wake, *Journal of Fluid Mechanics* 224 (1991) 77–90.
[11] J.R. Filler, P.L. Marston, W.C. Mih, Response of the shear layers separating from the circular cylinder to small amplitude rotational oscillations, *Journal of Fluid Mechanics* 231 (1991) 481–499.
[12] J.E. Ffowcs Williams, B.C. Zhao, The active control of vortex shedding, *Journal of Fluids and Structures* 3 (1989) 115–122.
[13] K. Roussopoulos, Feedback control of vortex shedding at low Reynolds numbers, *Journal of Fluid Mechanics* 248 (1993) 267–296.
[14] X.Y. Huang, Feedback control of vortex shedding from a circular cylinder, *Experiments in Fluids* 20 (1996) 218–224.
[15] A. Baz, M. Kim, Active modal control of vortex-induced vibrations of a flexible cylinder, *Journal of Sound and Vibration* 165 (1993) 69–84.
[16] L. Cheng, Y. Zhou, M.M. Zhang, Perturbed interaction between vortex shedding and induced vibration, *Journal of Fluids and Structures* 17 (2003) 887–901.
[17] M.M. Zhang, L. Cheng, Y. Zhou, Closed-loop-controlled vortex shedding from a flexibly supported square cylinder under different schemes, *Physics of Fluids* 16 (2004) 1439–1448.
[18] M. Provansal, C. Mathis, L. Boyer, Benard–von Kármán instability: transient and forced regimes, *Journal of Fluid Mechanics* 182 (1987) 1–22.
[19] Y. Zhou, H.J. Zhang, M.W. Liu, The turbulent wake of two side-by-side circular cylinders, *Journal of Fluid Mechanics* 458 (2002) 303–332.
[20] B.M. Copeland, J.D. Buckley, R.G. Bryant, R.L. Fox, R.F. Hellbaum, THUNDER—an ultra-high displacement piezoelectric actuator, NASA Langley Research Center, Hampton, VA, 1999, 23681–0001.
[21] W. Jin, Y. Zhou, P.K.C. Chan, H.G. Xu, A fibre-optic grating sensor for the study of flow-induced vibrations, *Sensors and Actuators* 79 (2000) 36–45.
[22] M.M. Zhang, Y. Zhou, L. Cheng, Closed-loop-manipulated wake of a stationary square cylinder, *Experiments in Fluids* 39 (2005) 75–85.
[23] B.J. Cantwell, D. Coles, An experimental study of entrainment and transport in the turbulent near wake of a circular cylinder, *Journal of Fluid Mechanics* 136 (1983) 321–374.
[24] Y. Zhou, R.A. Antonia, Critical points in a turbulent near-wake, *Journal of Fluid Mechanics* 275 (1994) 59–81.
[25] R.A. Antonia, S. Rajagopalan, A comment on the determination of drag of a circular cylinder, *AIAA Journal* 28 (1990) 1833–1835.
[26] B.E. Lee, The effect of turbulence on the surface pressure field of a square prism, *Journal of Fluid Mechanics* 69 (1975) 263–282.
[27] H. Sakamoto, H. Haniu, Y. Kobayashi, Fluctuating force acting on rectangular cylinders in uniform flow (on rectangular cylinders with fully separated flow), *Transactions JSME Series B* 55 (1989) 2310–2317.
[28] Y. Zhou, R.A. Antonia, Effect of initial conditions on structures in a turbulent near-wake, *AIAA Journal* 32 (2002) 1207–1213.
[29] H.J. Zhang, Y. Zhou, R.A. Antonia, Longitudinal and spanwise structures in a turbulent wake, *Physics of Fluids* 12 (2000) 2954–2964.
[30] Y. Zhou, Z.J. Wang, R.M.C. So, S.J. Xu, W. Jin, Free vibrations of two side-by-side cylinders in a cross-flow, *Journal of Fluid Mechanics* 443 (2001) 197–229.